Supporting information

A "competitive occupancy" strategy toward Co-N_4 single-atom catalysts embedded in 2D TiN/rGO sheets for high-efficient and stable aromatic nitroreduction

Ying Gu,[a] Aiping Wu,[b] Lei Wang,[b] Dongxu Wang,[b] Haijing Yan,[b] Peng Yu,[b] Ying Xie,[b] Chungui Tian,*[b] Fanfei Sun[c] and Honggang Fu*[ab]

[a]*Key Laboratory of Superlight Materials and Surface Technology of Ministry of Education, College of Materials Science and Chemical Engineering, Harbin Engineering University, Harbin 150001, P. R. China. E-mail: fuhg@hlju.edu.cn, fuhg@vip.sina.com;*

[b]*Key Laboratory of Functional Inorganic Material Chemistry, Ministry of Education of the People's Republic of China, Heilongjiang University. Harbin 150080, China chunguitianhq@163.com, tianchungui@hlju.edu.cn.*

[c]*Shanghai Synchrotron Radiation Facility (SSRF) Shanghai Institute of Applied Physics, Chinese Academy of Sciences, Shanghai 201204, China;*

Table S1. The samples and their corresponding preparation conditions.

Name	m [$Co(NO_3)_2 \cdot 6H_2O$]	V_{TBOT}	m_{GO}
TiN/rGO	0 mg	3 mL	0.1 g
Co_4N-rGO	10 mg	0 mL	0.1 g
Co-N_4/TiN-rGO	10 mg	3 mL	0.1 g
Co-N/rGO-Ti-1.5	10 mg	1.5 mL	0.1 g
Co-N/rGO-Ti-3	10 mg	3 mL	0.1 g
Co-N/rGO-Ti-6	10 mg	6 mL	0.1 g

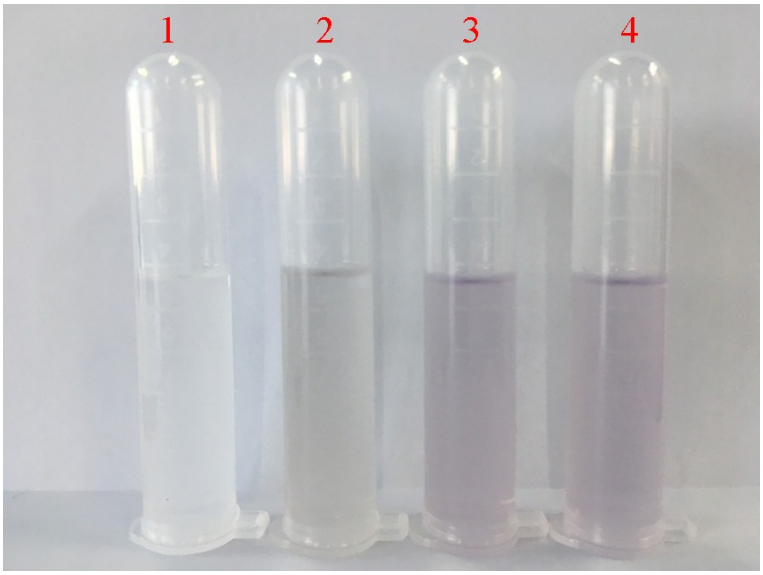

Figure S1. The photograph of the supernatant obtained by centrifugation after the addition of Co precursor (10 mg) into GO dispersion for 12 hours in the presence of different amount of TBT (0, 1.5, 3, 6 mL from left to right).

As shown in Figure S1, without TBT, the supernatant have no distinct color, indicating the complete combination of Co^{2+} with GO. By adding 1.5 ml Ti source, the supernatant shows a pale pink color, implying the little combination of Co^{2+} with GO. The presence of 3 mL (6 mL) of TBT leads to deeper color of supernatant close to the original ones, indicating the

combination of trace Co^{2+} with supports. The results show that we can control the amount of Co species on GO by “competitive occupancy” of Ti species.

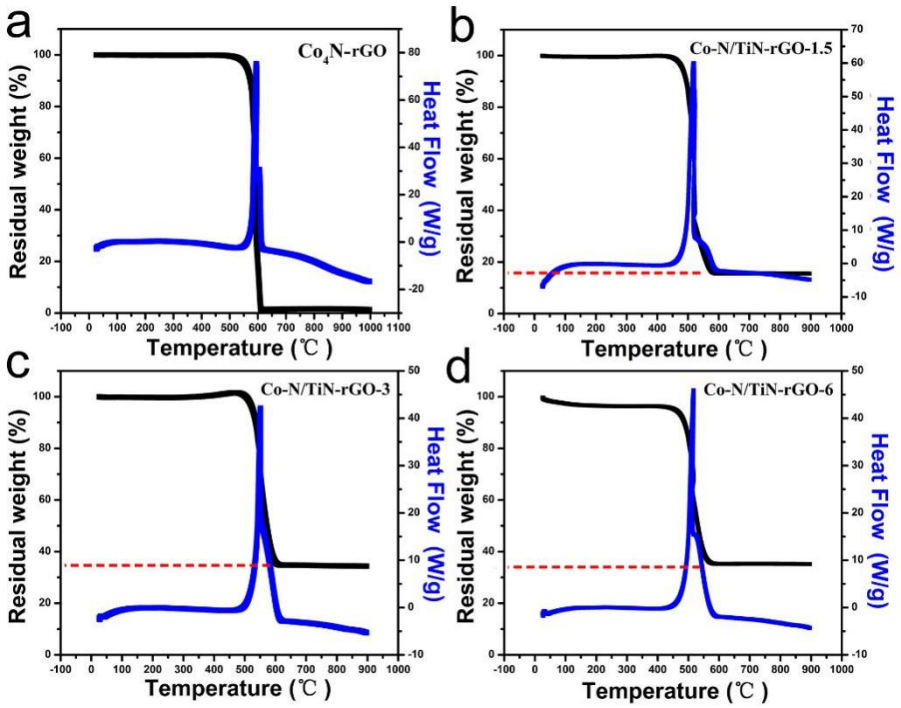

Figure S2. TG curves of the Co_4N-rGO, Co-N/rGO-Ti-1.5, Co-N/rGO-Ti-3 and Co-N/rGO-Ti-6, respectively (under air atmosphere).

Table S2. The elemental compositions of the samples calculated based on TGA and ICP measurements.

***S*ample**	V_{TBOT}	$m_{Co(NO3)2\cdot 6H2O}$	**The content of TiN**	**The content of Co（ICP）**	$m_{Co}:m_{total\ mass}$	$m_{Co}:m_{rGO}$
Co_4N-rGO	0 mL	10 mg	0%	6.44 μg/mL	2.576%	2.46%
Co-N/rGO-Ti-1.5	1.5 mL	10 mg	12.8%	1.07 μg/mL	0.428%	0.49%
Co-N/rGO-Ti-3	3 mL	10 mg	26.6%	0.34 μg/mL	0.136%	0.185%
Co-N/rGO-Ti-6	6 mL	10 mg	27.31%	0.2 μg/mL	0.08%	0.11%

*Ti content were detected by TGA, and Co content was determined by ICP.

We have determined quantitative results of TiN and Co for Co_4N-rGO, Co-N/rGO-Ti-1.5, Co-N/rGO-Ti-3 and Co-N/rGO-Ti-6 based on TG and ICP analyses (Figure S2 and Table S2). From TG test in air, we can see a loss weight of sample at ~500°C, which can be ascribed to combined results from the decomposition of rGO and oxidation of TiN. During the calcination, the TiN in the composites can be converted into TiO_2 in company with the formation of carbon oxide gases by the reaction of the carbon with O_2. The carbon oxide gases are released and TiO_2

stay as solid in the system (crucible). As determined by TG analysis, the amount of TiO_2 for Co-N/TiN-rGO-1.5, Co-N/TiN-rGO-3 and Co-N/TiN-rGO-6 is about 16.5 wt%, 34.4 wt% and 35.3 wt%, respectively (Figure S2). Thus, we can estimated the content of TiN in the composites based on the amount of TiO_2. The content of TiN in Co-N/TiN-rGO-1.5, Co-N/TiN-rGO-3 and Co-N/TiN-rGO-6 is approximate to 12.8 wt%, 26.6% and 27.31 based on the below equation:

$$\mathbf{TiN\%=TiO_2\%\times 61.8/79.9}$$

Obviously, the amount of Ti species on final samples increases with the increase of TBT amount, and the amount of Ti species is close to saturation when 3 mL of TBT is added. The less occupancy of Ti species, the more residual of functional group on GO and vice versa. The inductively coupled plasma optical emission spectrometry (ICP-OES) analysis revealed that the amount of Co in final sample was 0.428 wt%, 0.136 wt% and 0.08%, corresponding to the use of 1.5 mL, 3 mL, and 6 mL TBT. The results show that the amount of Co species on GO can be well controlled by “competitive occupancy” of Ti species.

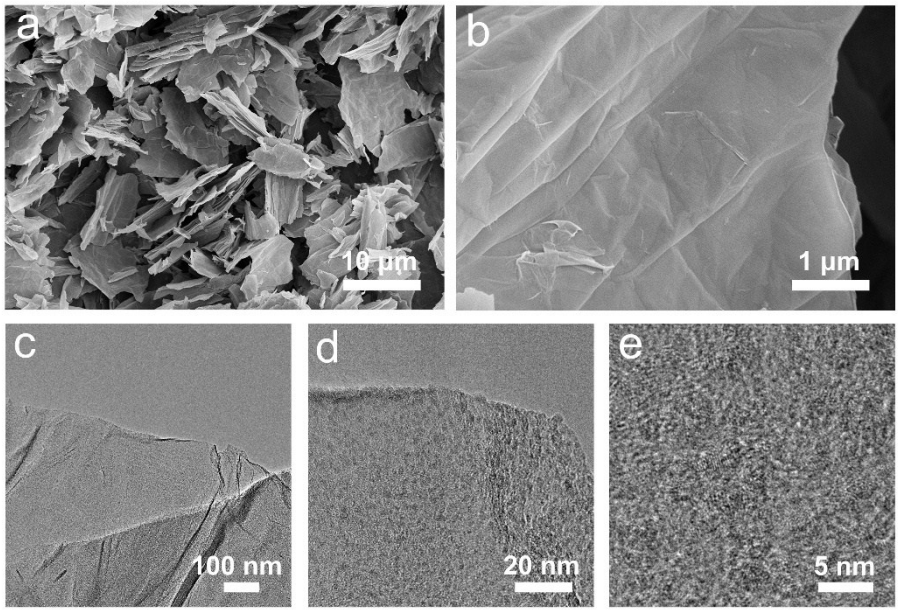

Figure S3. SEM and TEM images of the precursor of Co-N_4/TiN-rGO sample.

The morphology of the precursor of Co-N_4/TiN-rGO sample after hydrothermal treatment were investigated by SEM and TEM. As shown in Figure S3a and S3b, the scanning electron microscopy show that the precursor exhibits the thin sheets structure similar to that of GO which implying the small size and uniform distribution of Ti-species on rGO. The TEM images also reveale the ultra-thin layer structure of the sample and it can be obviously seen that there are some dense and uniform particles (~5 nm) on rGO.

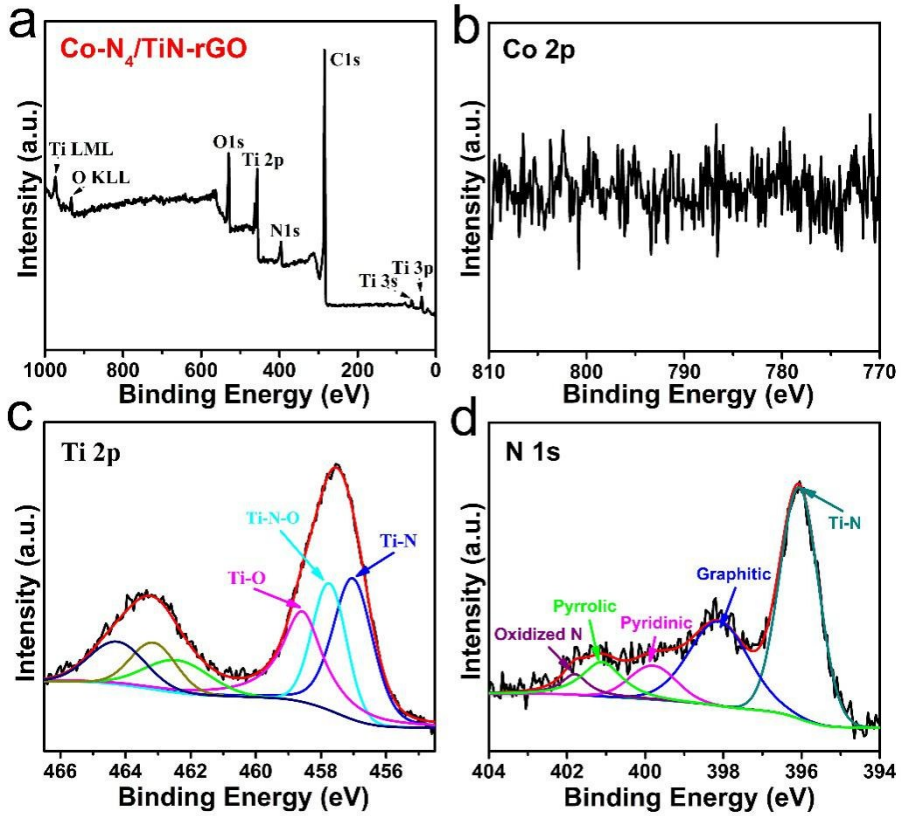

Figure S4. (a) XPS survey spectrum of Co-N_4/TiN-rGO and the high-resolution spectra of (b) Co 2p, (c) Ti 2p and (d) N 1s.

X-ray photoelectron spectroscopy (XPS) were collected to study the elemental composition and valence. As shown in Figure S4a, the survey spectrum of Co-N_4/TiN-rGO shows four peaks centered at 284.8, 396.4, 458.4, and 530.2 eV, corresponding to C 1s, N 1s, Ti 2p, and O 1s, respectively. The high resolution Co 2p spectra in Figure S4b shows no obvious peak of Co element, which should be ascribed to the low content exceeding the detection limit of our XPS. The core level Ti 2p spectrum (Figure. S4c) can be divided into 6 peaks (three pairs of spin-orbit split doublets), which are Ti-N (2p $_{3/2}$ at 455.7 eV, 2p $_{1/2}$ at 461.8 eV), Ti-N-O (2p $_{3/2}$ at 456.9 eV and 2p $_{1/2}$ at 463.2 eV), and Ti-O (2p $_{3/2}$ at 458.5 eV and 2p $_{1/2}$ at 464.4 eV). The presence of Ti-N-O and Ti-O should be due to the slight surface oxidation of nitrides during handling. The High resolution N 1s spectrum (Figure. S4d) was divided into several characteristic peaks at 398.2 (graphitic N), 399.8 (pyridinic N), 401.1 (pyrrolic N), and 401.8 eV (N-O), respectively, which indicates the doping of N in carbon. The strong peak located at 396.1 eV is assigned to N-Ti. The existence of C-N bonding in C1s spectrum also indicated the doping of N into the carbon. X-ray photoelectron spectroscopy (XPS) shows the formation of

TiN and N-doped rGO, but with no obvious sign of Co element, which should be ascribed to the low content exceeding the detection limitation of XPS.

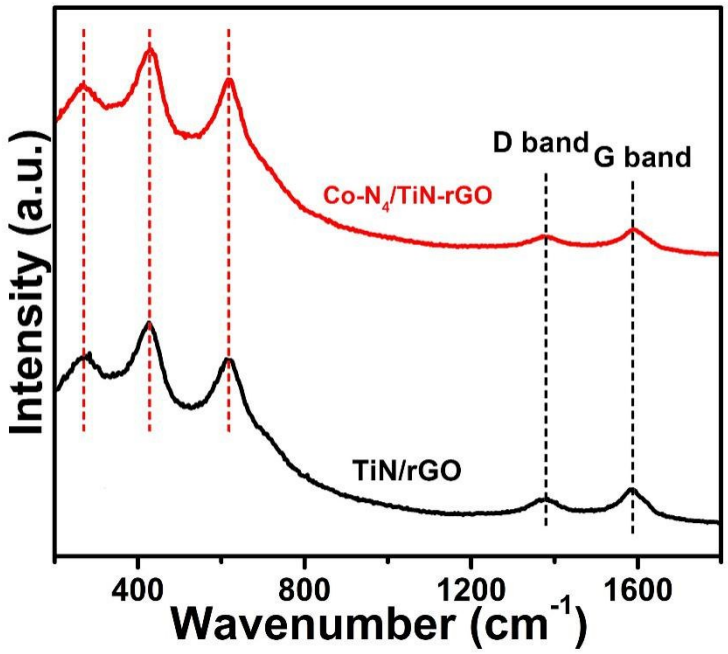

Figure S5. Raman spectra of the Co-N_4/TiN-rGO and TiN/rGO catalysts.

The structure of the Co-N_4/TiN-rGO is further confirmed by Raman spectroscopy. As shown in Figure S5, two well-defined peaks displayed at 1375 and 1590 cm^{-1} are assigned to the D and G peaks of GO, respectively. In addition, peaks positioned at around 266, 429 and 620 cm^{-1} are corresponding to bonds in TiN. Raman spectra show the presence of Ti-N and carbon (rGO) in Co-N_4/TiN-rGO sample. The similar Raman peaks for the Co-N_4/TiN-rGO and TiN/rGO indicated the little effect of dispersed Co species on the structure of TiN/GO.

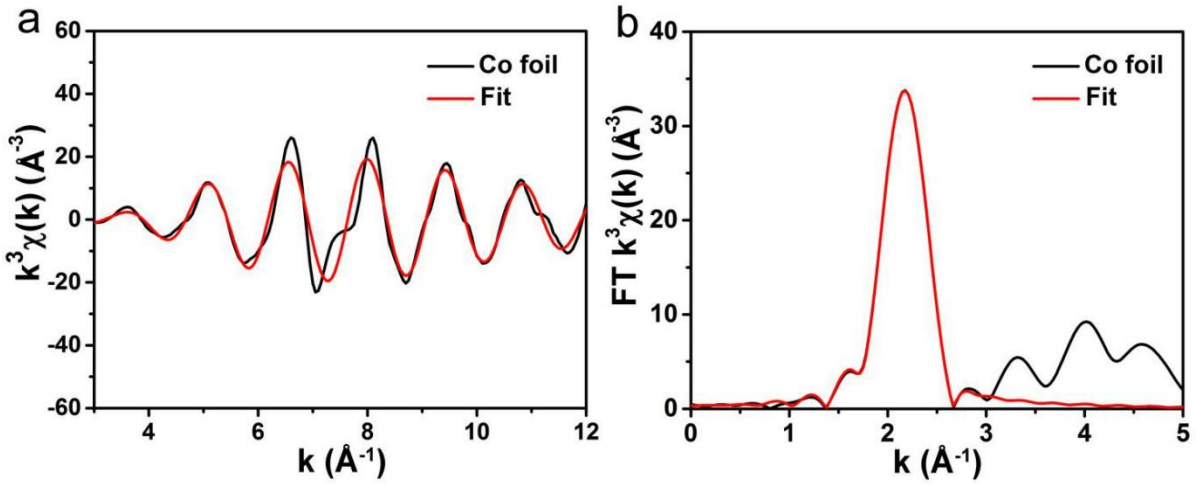

Figure S6. The corresponding EXAFS fitting curves of Co foil at (a) k space and (b) R space, respectively.

Table S3. Structural parameters of Co-N_4/TiN-rGO and Co foil extracted from the EXAFS fitting.

Sample	Path	C.N.	R (Å)	$\sigma^2\times10^3$ (Å^2)	ΔE (eV)	R factor
Co foil	Co-Co	12*	2.49±0.01	6.3±0.1	7.3±0.2	0.001
Co-N_4/TiN-rGO	Co-N	4.4±1.0	1.86±0.01	4.1±1.8	-7.8±3.3	0.007

C. N. is the coordination number; R is interatomic distance (the bond length between central atoms and surrounding coordination atoms); $\sigma^2\times10^3$ is Debye-Waller factor (a measure of thermal and static disorder in absorber-scatter distances); ΔE is edge-energy shift (the difference between the zero kinetic energy value of the sample and that of the theoretical model). R factor is used to value the goodness of the fitting.

Table S3 summarizes the fitting results of the EXAFS spectra of Co-N_4/TiN-rGO and Co foil. EXAFS fitting was performed to obtain the structural parameters and take out the quantitative chemical configuration of Co atoms. The first shell of the Co atoms in Co-N_4/TiN-rGO exhibits a coordination number of 4.4 and the mean bond length is 1.86 Å. The analyses indicate that Co atoms are coordinated by four N atoms.

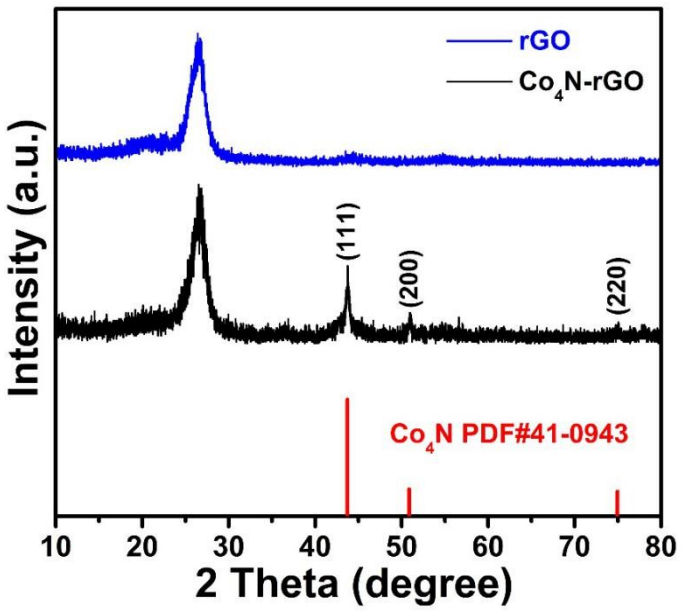

Figure S7. The XRD pattern of rGO and Co_4N-rGO (the nitridation is 800^{o}C and time is 2 h).

The crystalline structure of Co_4N-rGO prepared by nitridation of the precursor from the use of 10 mg of $Co(NO_3)_2$ in the absence of TBT and rGO was analyzed by XRD. It can be observed from Figure S7 that the XRD pattern of rGO exhibits a broad peak at 26^o, which is well indexed to the (002) reflection of hexagonal graphite. For Co_4N-rGO, the main peaks at around 43.7^o, 50.8^o and 74.9^o can be indexed to Co_4N (JCPDS card: no. 41-0943). The results showed that without the "competitive occupancy" by Ti species, a large amount of Co^{2+} can combine with GO, thus resulting the formation of large Co_4N particles.

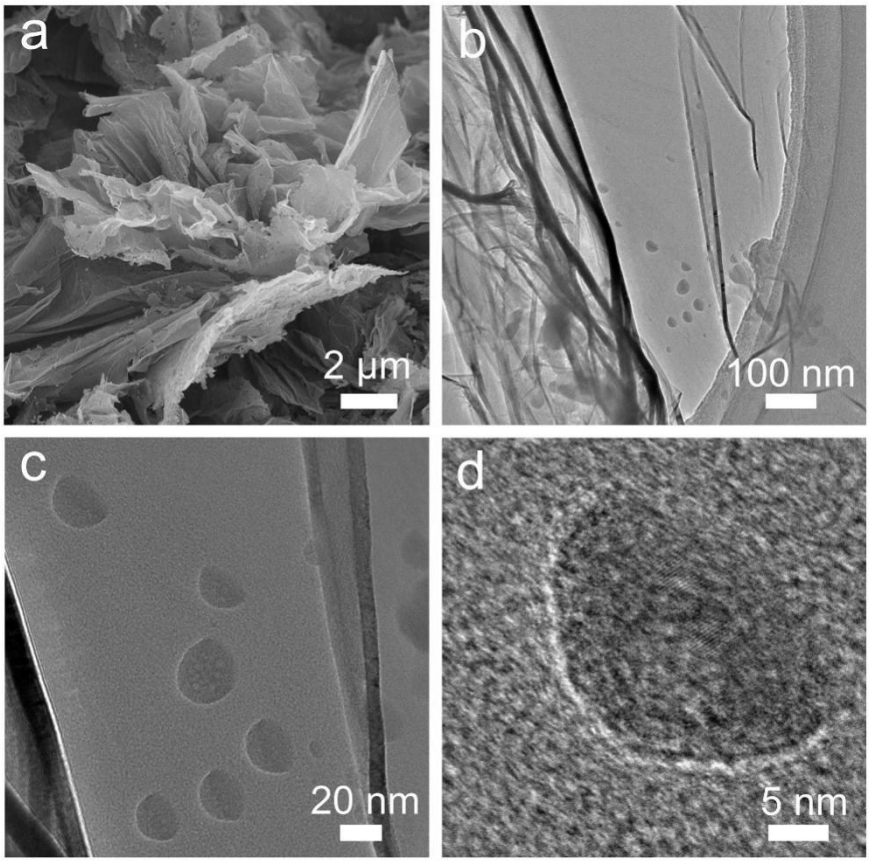

Figure S8. SEM and TEM images of the Co_4N-rGO sample.

The morphology of Co_4N-rGO were investigated by SEM and TEM. As shown in Figure S8a, the Co_4N-rGO still maintain the two-dimensional structure similar to GO. However, a significant aggregation of the particles can be observed on the surface of rGO. The TEM images of Co_4N-rGO (Figure S8b-S8d) further exhibit that large Co_4N nanoparticles (about 20 nm) are grown on rGO sheet. The TEM, SEM and XRD further indicates the key role of "competitive occupancy" by Ti species to the synthesis of Co-N_4 SACs on support.

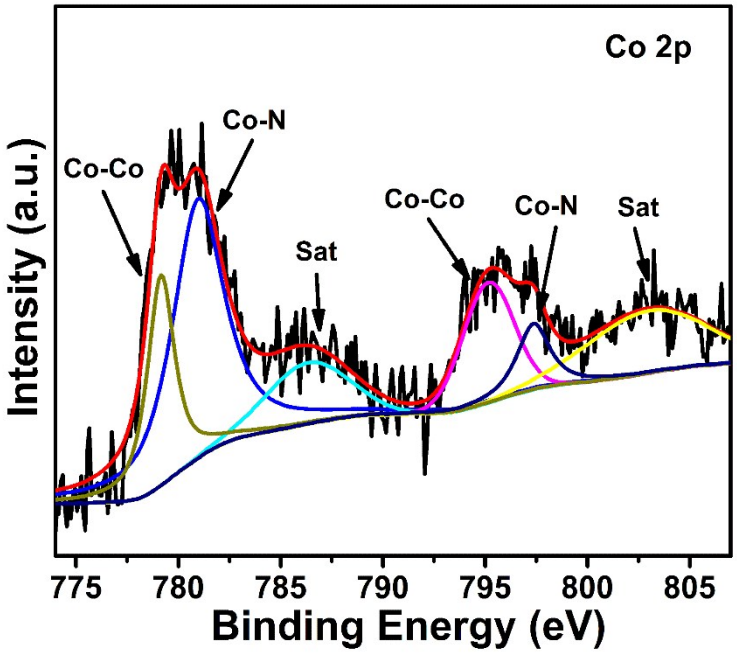

Figure S9. The high-resolution XPS spectrum of Co 2p of Co_4N-rGO.

To probe the chemical and electronic states of Co_4N-rGO, XPS were further performed. The Co 2p XPS spectrum of Co_4N (Figure S9) displays multiple broad peaks, suggesting more than one chemical states of Co in Co_4N. By carefully fitting the Co 2p, the peaks located at 779.3 and 795.2 eV are assigned to the Co $2p_{3/2}$ and Co $2p_{1/2}$ of the Co-Co, while the peaks centered at 781 and 797.3 eV correspond to Co-N bonds in Co_4N.[1]

[1] Z. Y. Chen, Y. Song, J. Y. Cai, X. S. Zheng, D. D. Han, Y. S. Wu, Y. P. Zang, S. W. Niu, Y. Liu, J. F. Zhu, X. J. Liu, G. M. Wang, *Angew. Chem. Int. Ed.* **2018**, *57*, 5076-5080.

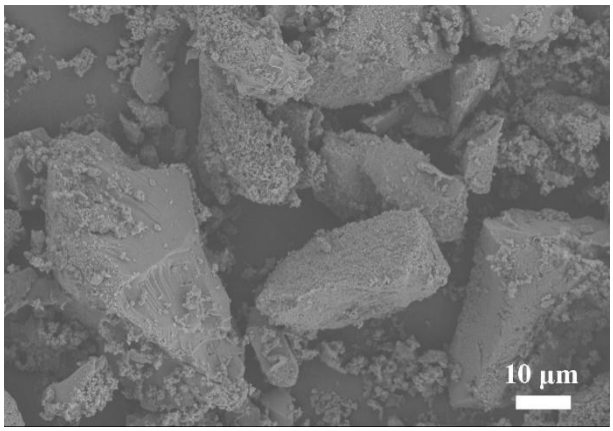

Figure S10. SEM image of the sample prepared by using distilled water as solvent.

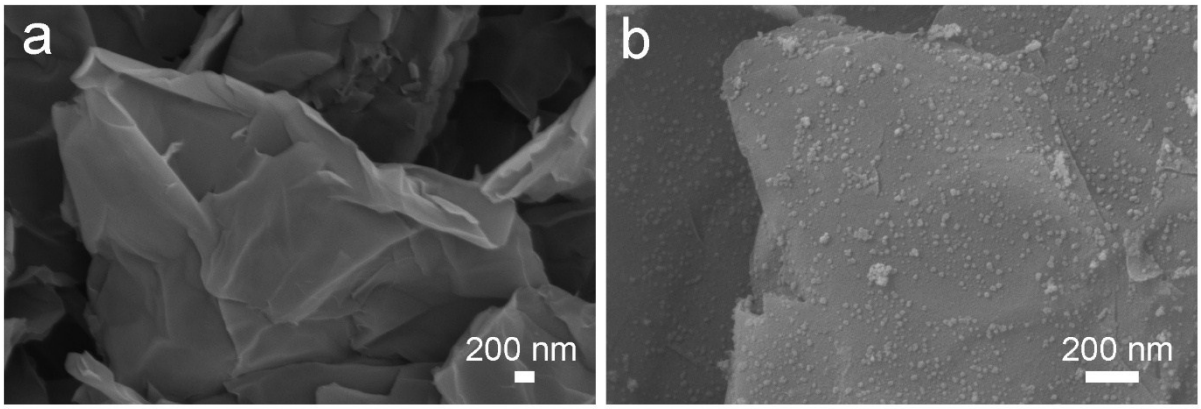

Figure S11. SEM images of the samples prepared using cyclohexane (a) and absolute ethanol (b) as solvents, respectively.

There are several keys for the formation of the Co SACs on TiN-GO supports. The combination of TBT on GO can be effected by solvent used in the synthesis. Figure S10 shows the SEM image of the samples prepared by using the distilled water as the solvent but not cyclohexane. We can see the formation of the large block material in this case, which should be due to the rapid hydrolysis of the tetrabutyl titanate in water. The result indicates the importance of controlling solvent kind to realize uniform growth of Ti-O species on rGO. The use of non-polar cyclohexane is favorable to form uniform and dense small particles on GO (Figure S11a), while the use of ethanol can result in the formation of larger TiN particles on GO as shown in Figure S11b. The difference should be relative with the different polarization of cyclohexane and ethanol that effect the combination of GO with Ti and Co species.

Table S4. ICP test results of Co-N_4/TiN-rGO samples after 15 catalytic cycles.

***S*ample**	**The content of TiN**	**The content of Co（ICP）**
Co-N_4/TiN-rGO	26.6%	1.07 μg/mL
Co-N_4/TiN-rGO-after	25.8%	1.02 μg/mL

After 15 catalytic cycles, the used catalyst named Co-N_4/TiN-rGO-after was collected and analyzed by ICP-OES. As shown in Table S4, there is almost no change in Co loading after 15 cycles of catalytic cycling with the fresh sample.

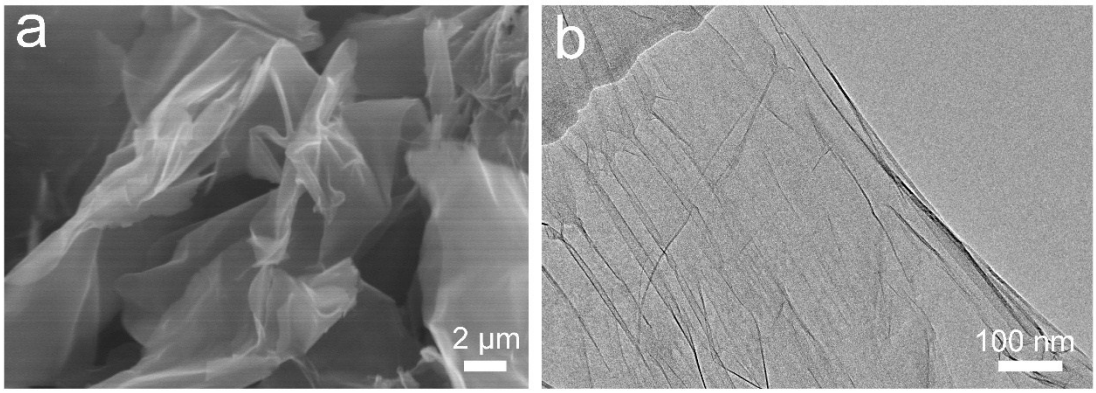

Figure S12. (a) SEM and (b) TEM photos of Co-rGO-1 catalyst.

The morphology of Co-rGO-1 were investigated by SEM and TEM. As shown in Figure S12, the Co-rGO-1 still maintain the two-dimensional structure similar to GO. The Co species are undetectable by SEM and TEM due to the low content of Co.

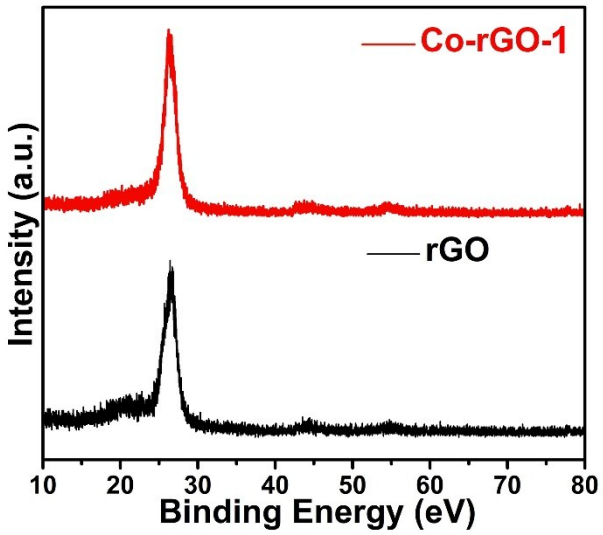

Figure S13. XRD patterns of Co-rGO-1 and rGO.

The XRD patterns (Figure S13) show that the Co-rGO-1 holds a broad diffraction peak locating at around 26°, which is well indexed to the (002) reflection of hexagonal graphite. No diffraction peaks of cobalt species are observed, ascribing the low amount of Co species.

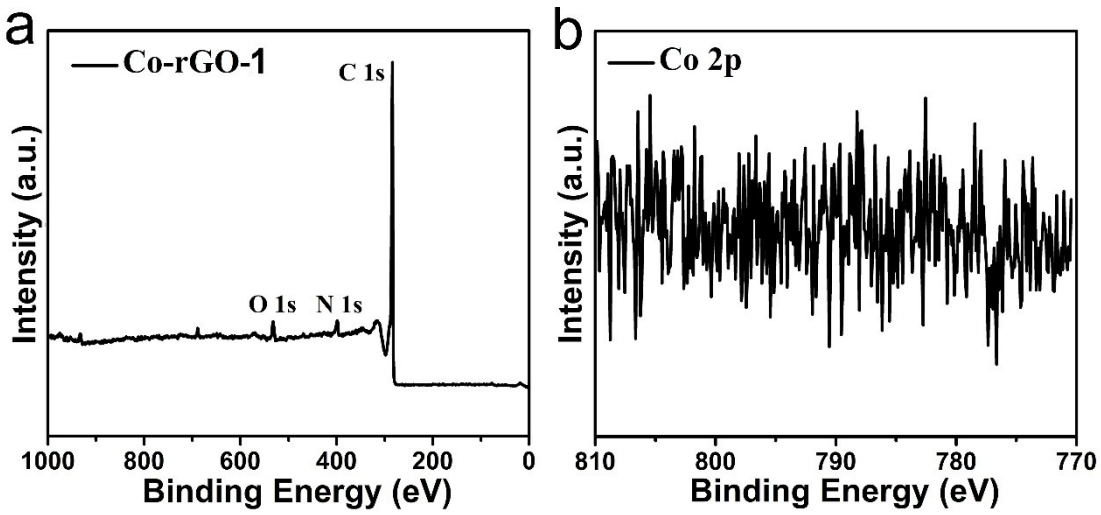

Figure S14. (a) XPS scan spectrum of Co-rGO-1 and (b) high-resolution spectrum of Co 2p.

To further ascertain the element composition and chemical bonding state of catalyst, X-ray photoelectron spectroscopy (XPS) data were collected. As shown in Figure S14, the XPS survey

spectrum shows three peaks centered at 284.8, 396.4, and 530.2 eV, corresponding to C 1s, N 1s, and O 1s, respectively. There is no obvious peak of Co element, which should be due to its low content.

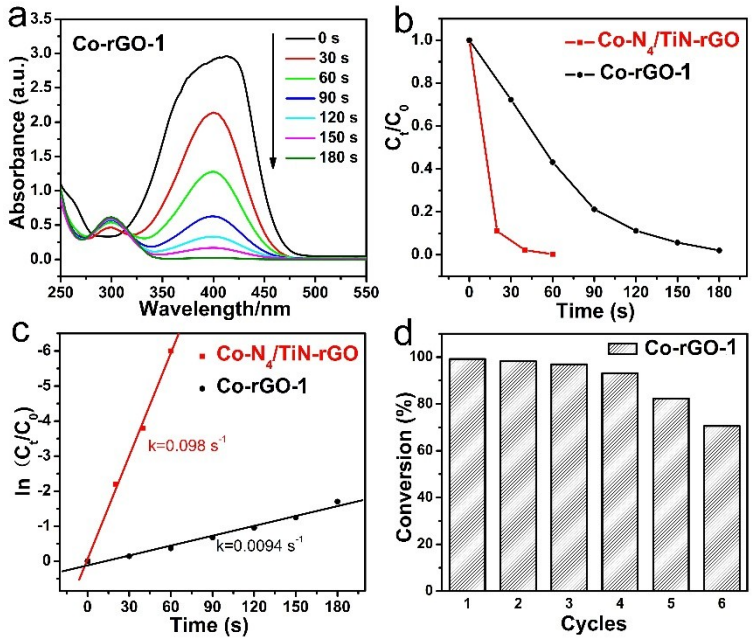

Figure S15. (a)The change of absorption value for 4-NP solution at 400 nm in the presence of $NaBH_4$ over Co-rGO-1; (b) C/C_0 and (c) $\ln(C/C_0)$ as a function of reaction time, and (d) reused activity and Co-rGO-1.

The Co-rGO-1 is used as catalyst for the reduction reaction of 4-nitrophenol. As shown in Figure S15a, much longer reaction time was required over Co-rGO-1 (180 s) by the comparison with that over Co-N_4/TiN-rGO (60 s) under similar conditions. The plot of C_t/C_0 and $\ln(C_t/C_0)$ against reaction time is shown in Figure S15b and S15c. The rate constant (k_1) of the reaction was calculated as 0.098 s^{-1} and 0.0094 s^{-1} for the Co-N_4/TiN-rGO and Co-rGO-1 catalysts, respectively. Notably, the Co-rGO-1 catalyst shows a significant decrease in catalytic performance after 4 cycles (Figure S15d). However, for Co-N_4/TiN-rGO, the conversion is still reached almost 100% of first run even after 15 cycles (Figure 3h). The good reused ability of Co-N_4/TiN-rGO can be ascribed to the role of TiN as "spacer". In another word, the Co-N_4 SACs on GO are surrounded and separated by TiN, which effectively hinders their migration and aggregation during the catalysis.

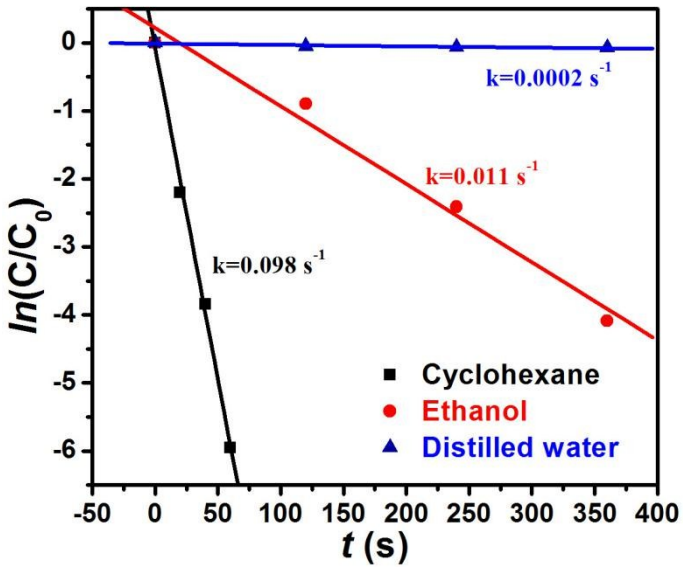

Figure S16. The comparison of catalytic performance of different catalysts prepared by using distilled water, ethanol and cyclohexane as solvents during the "competitive occupancy" step (the synthesis of precursor).

The solvent used during the "competitive occupancy" step (the synthesis of precursor) has obvious effect on the performance of final catalysts. As shown in Figure S16, the catalyst prepared by using water and ethanol as solvent during the "competitive occupancy" step shown poor performance than those in cyclohexane. The results should be relative with the large size and poor dispersion of TiN in the case of using water and ethanol as solvent, which result in an ineffective separation and stability of Co species.

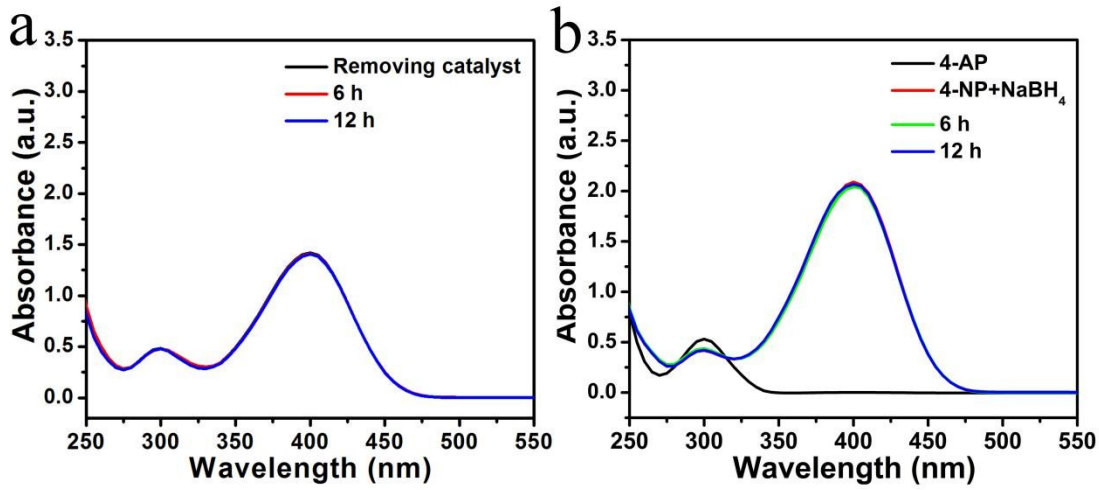

Figure S17. (a) The change of UV-vis absorption spectra for the solution fromremoving Co-N_4/TiN-rGO after reaction 10 s, and additional standing for 6 h and 12 h; (b) The change of UV-vis absorption spectra for the solution from removing Co-N_4/TiN-rGO after reaction of 1 min (full conversion) and additional add of fresh 4-NP and $NaBH_4$ in the solution.

We have performed additional experiments to obtain additional information about the heterogeneity or homogeneity of the catalyst in the reaction. To this, the catalyst is take off from reaction system after reaction of a few seconds. In this case, there are still presence of residual 4-NP in the solution. After standing the solution for more than 12 h, there are no obvious change in UV-vis adsorption spectrum (Figure S17a). In another test, the conversion is first completed (no obvious peak about 4-NP is detected) and the catalyst was taken out. To this solution, the fresh 4-NP solution and $NaBH_4$ is added and an obvious absorption peak of 4-NP can be observed. After standing for more than 12 h, there was no change in absorption peak (Figure S17b). The experiments indicate that the conversion cannot be happen with no assistance of Co-N_4/TiN-rGO catalyst, further indicating the heterogeneous catalytic characteristics.

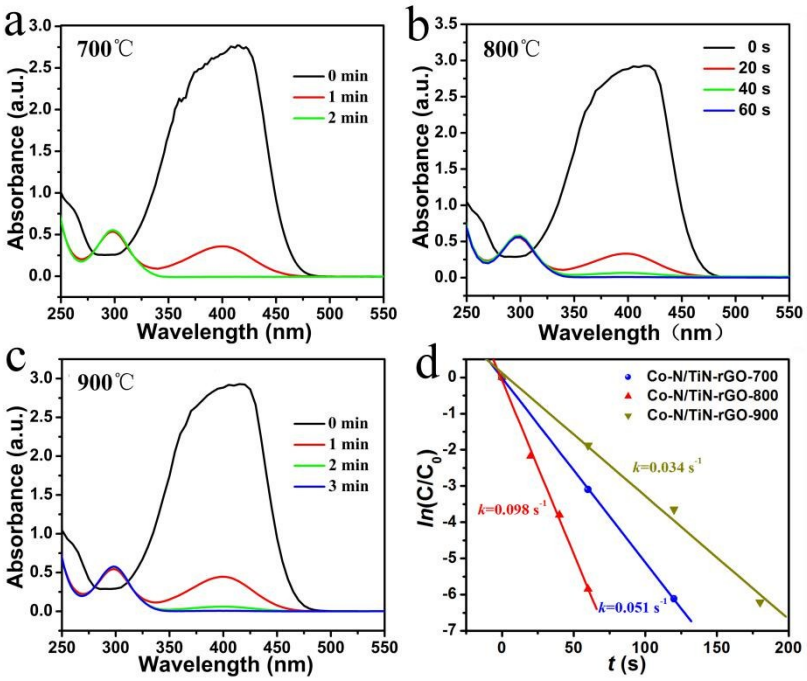

Figure S18. The change in absorbance at 400 nm for a 4-NP solution at 25°C catalyzed by samples from different calcined temperatures.

The precursor were calcinated under NH_3 atmosphere with a heating rate of 3°C min^{-1} at 700°C and 900°C and maintained at this temperature for 2 h, which are denoted as Co-N/TiN-rGO-700 and Co-N/TiN-rGO-900, respectively. The performance test results are shown in Figure S18. The conversion of the 4-NP was approximately 100% for Co-N/TiN-rGO-700 and Co-N/TiN-rGO-900 at a reaction time of 2 min and 3 min, respectively. The apparent first-order rate constant (k) was approximately 0.034 s^{-1}, 0.098 s^{-1} and 0.051 s^{-1} for Co-N/TiN-rGO-700, Co-N/TiN-rGO-800 and Co-N/TiN-rGO-900, respectively. The Co-N_4/TiN-rGO (calcinated at 800°C) shows the highest catalytic activity, which indicates that a suitable treatment temperature is conducive to the formation of an efficient catalyst.

Table S5. The catalytic performance of Co-N_4/TiN-rGO for the conversion of 4-NP (0.3 mM) to 4-AP at different temperatures.

Catalytic reaction temperature (^oC)	45^oC	25^oC	15^oC	10^oC	5^oC
Time (min)	45 s	1 min	1 min	3 min	8 min

Table S6. The catalytic performance of Co-N_4/TiN-rGO for the conversion of different concentrations of 4-NP to 4-AP at 25^oC.

4-NP concentration	0.3 mM	1 mM	1.5 mM	2 mM
Time (min)	1 min	2 min	3 min	5 min

Besides good activity and stability, there are several virtues needing to be noted. First, the high activity of Co-N_4/TiN-rGO can make the fast conversion of 4-NP to 4-AP at low temperature. As shown in table S5, the catalyst can still convert 4-NP to 4-AP within 1 minute and 8 minute when the reaction temperature is 15^oC and 5^oC, respectively. The 4-NP could be completely transformed in 45 s as increase of reaction temperature to 45^oC. In addition, the high concentration of 4-NP can still be effectively converted within short time. The conversion of 1 mM, 1.5 mM, and 2 mM of 4-NP can reach 99% in 2 min, 3 min, and 5 min, respectively (Table S6).

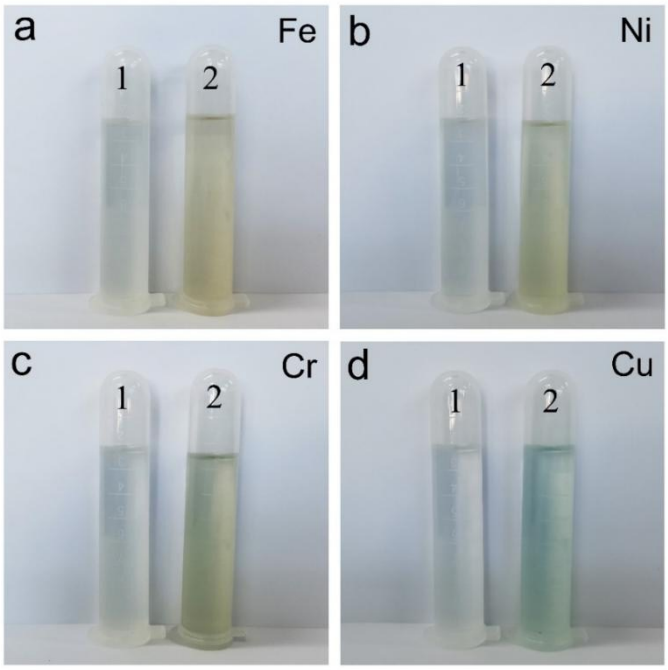

Figure S19. The photos of the supernatant obtained by centrifugation after adding different nitrates (Iron nitrate, nickel nitrate, chromium nitrate and copper nitrate) for 12 hours during the synthesis.

The competitive occupancy strategy used in this paper provides a feasible method for the simple synthesis of transition metal-based SACs (TM-SACs). We use four different nitrates (Fe, Ni, Cr, and Cu) in the synthesis process to verify the universality of the method. After stirring for 12 h, the dispersion was centrifuged to obtain a supernatant. Figure S19a shows the supernatant obtained by adding the same amount of iron nitrate (20 mg) during the synthesis process (labels 1 without TBT and labels 2 with TBT). Without TBT, the supernatant have no distinct color, indicating the complete combination of Fe^{3+} with GO. The adding 3 mL TBT can make a pale yellow color of the supernatant, implying the little combination of Fe^{3+} with GO. Figure S19b shows the supernatant obtained by adding the same amount of nickel nitrate (20 mg) during the synthesis process (labels 1 without TBT and labels 2 with TBT). Similarly, without TBT, the supernatant have no distinct color, indicating the complete combination of Ni^{2+} with GO. The adding 3 mL TBT can make a pale green color of the supernatant, implying the little combination of Ni^{2+} with GO. The same results were obtained with the use of chromium nitrate and copper nitrate in Figure S19c and Figure S19d. The results show that the competitive occupancy strategy adopted in this paper can be widely applied to a variety of TM-SACs, which is convenient for the preparation of the single-atom catalysts.

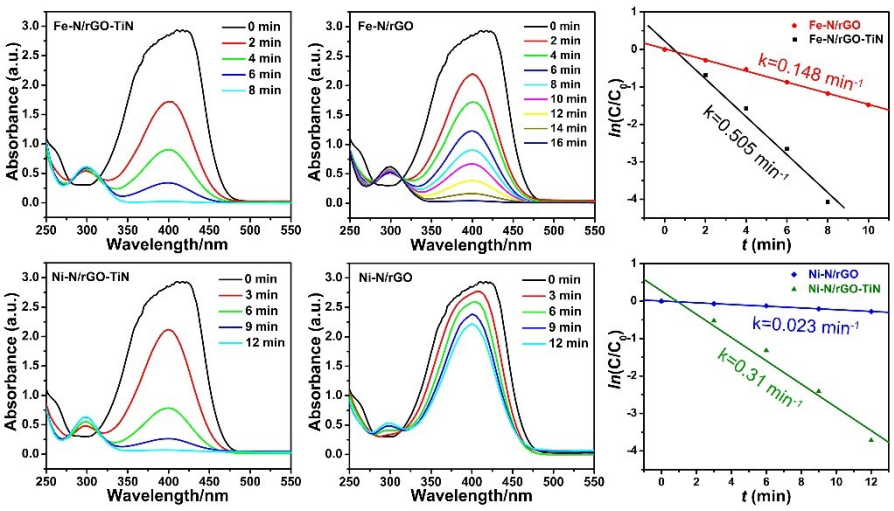

Figure S20. (a, b) The catalytic performance of Fe-N/TiN-rGO and Fe-N/rGO for the conversion of 4-NP to 4-AP; (c) $\ln(C/C_0)$ as a function of reaction time; (d,e) The catalytic performance of Ni-N/TiN-rGO and Ni-N/rGO for the conversion of 4-NP to 4-AP; (f) $\ln(C/C_0)$ as a function of reaction time.

The Ni (Fe, Cr, Cu)-based SACss (Ni-N/TiN-rGO; Fe-N/TiN-rGO; Cr-N/TiN-rGO and Cu-N/TiN-rGO) were also synthesized by the competitive occupancy of corresponding metal salts with TBT. For comparison, the corresponding large particle metal catalysts (Ni-N/rGO; Fe-N/rGO; Cr-N/rGO and Cu-N/rGO) were also synthesized without TBT. The catalytic activity of the prepared Fe-N/TiN-rGO and Ni-N/TiN-rGO catalysts was also tested by the conversion of 4-NP to 4-AP. As shown in Figure S20, the catalytic activity of M-N SACs catalysts synthesized by this method is better than that of the corresponding large particle metal catalyst.

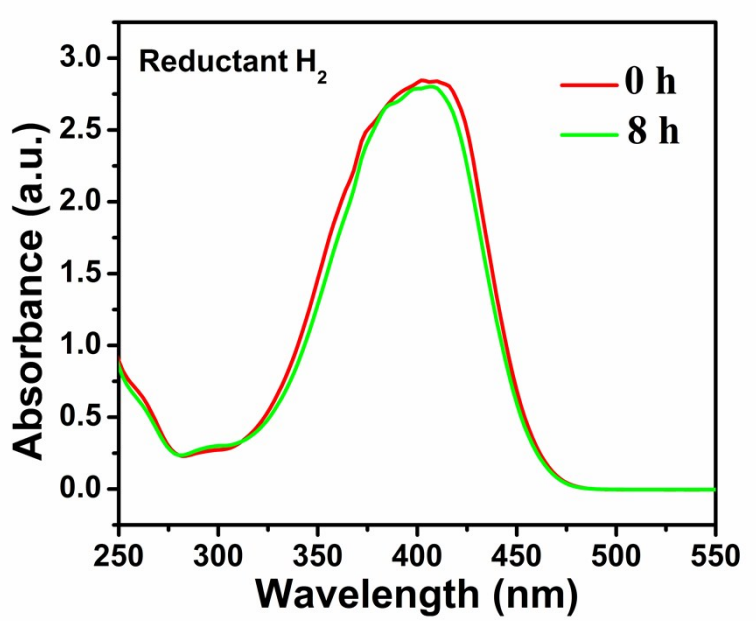

Figure S21. The change of absorption value for 4-NP solution at 400 nm in the presence of H_2 over Co-N_4/TiN-rGO. (120°C, 4 bar H_2)

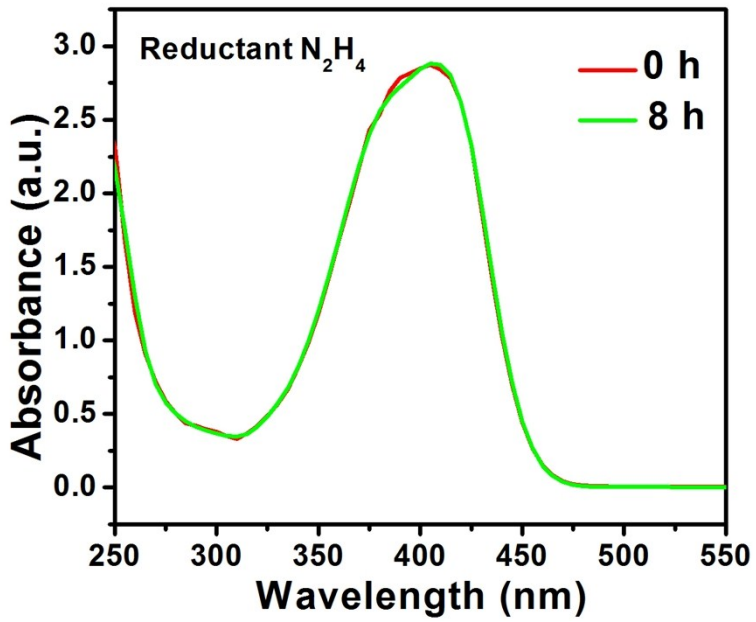

Figure S22. The change of absorption value for 4-NP solution at 400 nm in the presence of N_2H_4 over Co-N_4/TiN-rGO. (65°C, ethanol as solvent)

A wide range of reducing agents has been used for the catalytic transformation of nitroarenes to amines. Each of them possesses advantages and disadvantages with respect to their catalytic ability, cost as well as hazardousness. The performance test are carried out by using H_2 and

$N_2H_4 \cdot H_2O$ as the reducing agents. The results show that the Co-N_4/TiN-rGO catalyst has very little catalytic activity for aromatic nitroreduction with H_2 and $N_2H_4 \cdot H_2O$ as reducing agents (Figure S21 and Figure S22).

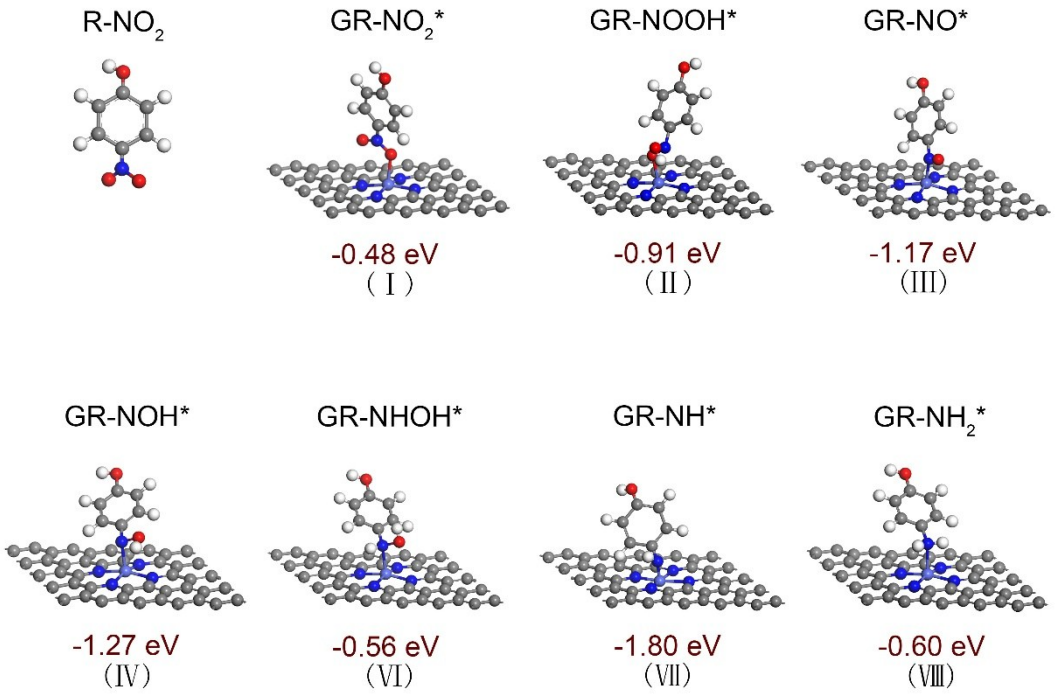

Figure S23. Detailed structures and relative energies of optimized geometries in 4-NP reduction processes.

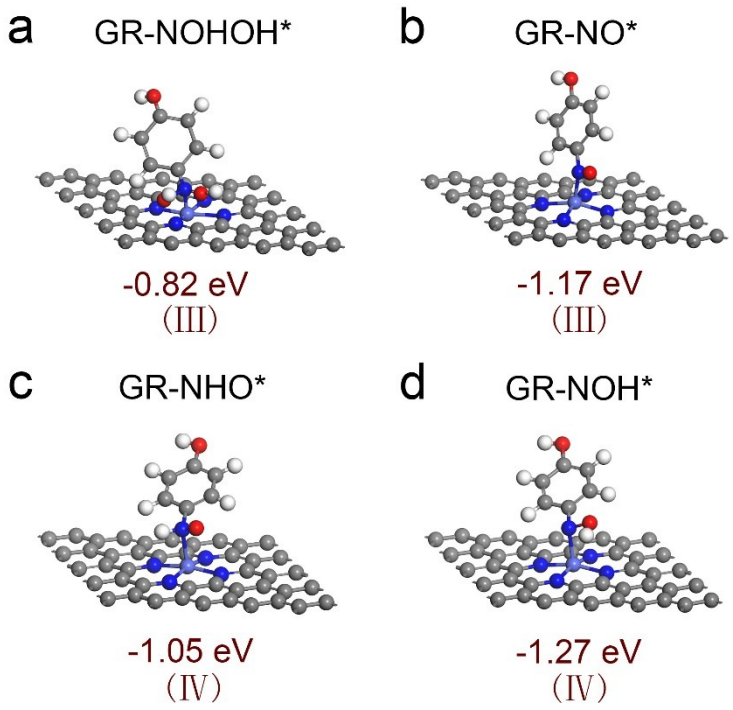

Figure S24. a and b are the detailed structures and optimized energies of the two intermediate products that may be obtained in the second step hydrogenation process. c and d are the detailed structures and optimized energies of the two intermediate products that may be obtained in the third step hydrogenation process.

Figure S23 and S24 show the detailed DFT model and intermediate products. According to the previous literatures, we calculate the adsorption energy of the possible reaction route for reducing nitroaromatics. The hydrogenation process are monitored by simulating the adsorption energies of the intermediates. The adsorption energy of 4-NP on Co-N_4/TiN-rGO (denoted as GR-NO_2^*) is -0.48 eV, where one of the oxygen in the nitro is attached to the single Co atom. The first hydrogen was added to the free oxygen in the nitro and the GR-NO_2^* was reduced to GR-$NOOH^*$. The adsorption energy of GR-$NOOH^*$ on Co-N_4/TiN-rGO is -0.91 eV, which is below the adsorption energy of 4-NP on Co-N_4/TiN-rGO. This proves that the first hydrogenation process is apt to occur on the surface of Co-N_4. For the addition of the second hydrogen, there are two different situations where the intermediates are GR-$NOHOH^*$ and GR-NO^*, respectively. The results show that the GR-NO^* has lower adsorption energy and is much more stable than GR-$NOHOH^*$. Therefore, during the hydrogenation process, the intermediate product is GR-NO^* instead of GR-$NOHOH^*$. For the third hydrogenation process, the calculations show that GR-NOH^* is more stable than GR-NHO^*. The fourth hydrogen is added to the oxygen of GR-NHO^* to form GR-$NHOH^*$, and the addition of the fifth hydrogen forms GR-NH^*. The last hydrogen is attached to the nitrogen of GR-NH^* to give the final product GR-NH_2^*.

Table S7. The comparison of catalytic performance of Co-N_4/TiN-rGO with other recently reported catalysts.

Catalysts	$c_{4\text{-NP}}$	Volume of solution	Amount of catalyst	c_{NaBH4}: $c_{4\text{-NP}}$	Rate constant	Time	Cycling stability	Reaction condition	Ref
Co-N_4/TiN-rGO	**0.30 mM**	**30 mL**	**5 mg**	**29:1**	**5.88 min^{-1}**	**1 min**	**15**	**25 °C**	**This work**
					0.6 min^{-1}	**8 min**		**5°C**	
	1.0 mM				**2.3 min^{-1}**	**2 min**		**25 °C**	
	2.0 mM				**1.2 min^{-1}**	**5 min**			
Pd@RCC_3	0.165mM	4 mL	-	400:1	1.25 min^{-1}	2 min	5	25 °C	Nat. Catal. **2018**, 1, 214-220
Cu_2O@ZIF-8	0.125	2.5 mL	30 mg	308:1	0.28 min^{-1}	30 min	-	25 °C	Angew. Chem. Int. Ed. **2018**, 57, 6834 -6837
PdCo@HZIF	0.154 mM	11 mL	0.03 mg	3583:1	-	2 min	5	Room temperature	Angew. Chem. Int. Ed. **10.1002/anie.201812827**
Au@NMOF-Ni	0.135 mM	11 mL	0.5 mg	67:1	0.404 min^{-1}	6 min	-	25 °C	Adv. Funct. Mater. **2018**, 28, 1802021
Pd1/GDY/G	0.095 mM	2 mL	0.015 mg	421:1	0.207 min^{-1}	3 min	10	Room temperature	Adv. Funct. Mater. **2019**, 1905423
PtNPs@COF	0.313 mM	2.3 mL	0.025 mg	693:1	-	8 min	6	Room temperature	J. Am. Chem. Soc. **2017**, 139, 17082-17088
Pd/GDYO	0.04 mM	2 mL	0.00125 mg	1075:1	0.322 min^{-1}	12 min	-	Room temperature	J. Am. Chem. Soc. **2015**, 137, 5260-5263
Au(5 nm)-γ-Fe_2O_3clusters	0.182 mM	44 mL	2 mg	40:1	2.43 min^{-1}	2 min	8	25 °C	Adv. Funct. Mater. **2017**, 1606215
S,N co-doped hollow carbon nanotubes	0.067 mM	3 mL	7.5 μL 1.25 mg/mL	298:1	0.106 min^{-1}	-	-	**0** °C	Adv. Mater. **2016**, 28, 10679-10683
					0.246 min^{-1}	10 min	-	20 °C	
Ni@GC	0.078 mM	2.5 mL	0.2 mg	1282:1	0.784 min^{-1}	5 min	5	25 °C	Small **2018**, 14, 1803188

Table S8. Reduction of various nitroarenes catalyzed by Co-N_4/TiN-rGO.

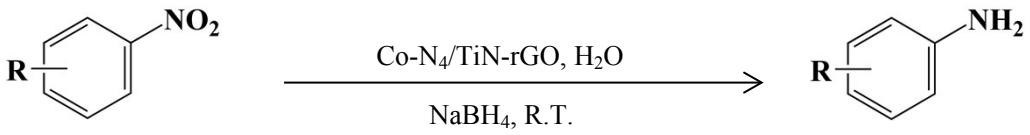

Entry	Substrate	Concentration	Product	Time(min)
1	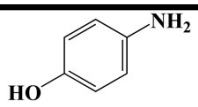	0.3 mM	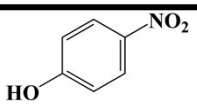	60 s
2	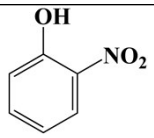	0.3 mM	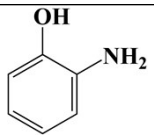	40 s
3	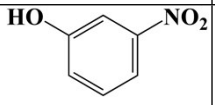	0.3 mM	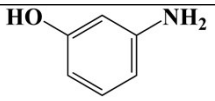	40 s
4	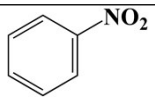	0.3 mM	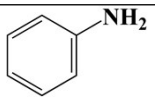	60 s
5	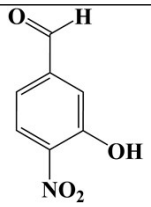	0.3 mM	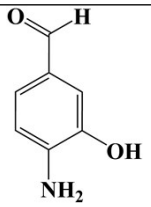	60 s
6	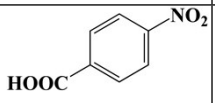	0.3 mM	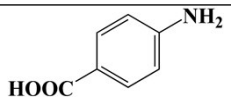	120 s
7	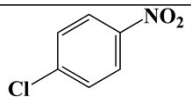	0.3 mM	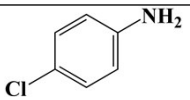	60 s

Reaction Conditions: c (aromatic nitro compounds): 0.3 mM. V (aromatic nitro compounds): 30 mL. m($NaBH_4$): 8 mg. m(catalyst): 5 mg. The solvent is distilled water or a mixed solution of distilled water and ethanol. Analysed by UV.